Aerosol Impacts on Thermally Driven Orographic Convection

ALISON D. NUGENT

National Center for Atmospheric Research, Boulder, Colorado

CAMPBELL D. WATSON

IBM T. J. Watson Research Center, Yorktown Heights, New York

GREGORY THOMPSON

National Center for Atmospheric Research, Boulder, Colorado

RONALD B. SMITH

Department of Geology and Geophysics, Yale University, New Haven, Connecticut

(Manuscript received 23 October 2015, in final form 30 April 2016)

ABSTRACT

Observations from the Dominica Experiment (DOMEX) field campaign clearly show aerosols having an impact on cloud microphysical properties in thermally driven orographic clouds. It is hypothesized that when convection is forced by island surface heating, aerosols from the mostly forested island surface are lofted into the clouds, resulting in the observed high concentration of aerosols and the high concentration of small cloud droplets. When trying to understand the impact of these surface-based aerosols on precipitation, however, observed differences in cloud-layer moisture add to the complexity. The WRF Model with the aerosol-aware Thompson microphysics scheme is used to study six idealized scenarios of thermally driven island convection: with and without a surface aerosol source, with a relatively dry cloud layer and with a moist cloud layer, and with no wind and with a weak background wind. It is found that at least a weak background wind is needed to ensure Dominica-relevant results and that the effect of cloud-layer moisture on cloud and precipitation formation dominates over the effect of aerosol. The aerosol impact is limited by the dominance of precipitation formation through accretion. Nevertheless, in order to match observed cloud microphysical properties and precipitation, both a relatively dry cloud layer and a surface aerosol source are needed. The impact of a surface aerosol source on precipitation is strongest when the environment is not conducive to cloud growth.

1. Introduction

Orographic clouds form daily over the island of Dominica in the Caribbean but they do not always form rain. Observations from the Dominica Experiment (DOMEX; Smith et al. 2012) indicate that high aerosol concentration, and clouds with high cloud droplet number concentration and small cloud droplet diameter, correlate well with a reduction in rainfall. The present study examines the role of a surface aerosol source in thermally driven orographic convection and precipitation formation in warm clouds.

a. Aerosol–cloud interactions

For decades it has been known that aerosols have an influence on cloud microphysical properties and precipitation formation (Twomey 1974; Albrecht 1989). These effects are termed aerosol–cloud interactions and the exact nature of the influence remains uncertain and highly contentious (Boucher et al. 2013).

A few aspects are certain. Aerosols are ubiquitous throughout the atmosphere, and their composition and number concentration vary depending on many factors including location, land use, and wind speed (Boucher et al. 2013; Huang et al. 2010; Adams and Seinfeld 2002;

Corresponding author address: Alison D. Nugent, National Center for Atmospheric Research, 3450 Mitchell Ln., Boulder, CO 80301.
E-mail: nugent@ucar.edu

DOI: 10.1175/JAS-D-15-0320.1

Rogers and Yau 1989). Aerosols are important to warm cloud formation because they act as cloud condensation nuclei (CCN), tiny suspended particles upon which water can condense to form cloud droplets (Rogers and Yau 1989). Since the 1970s it has been known that the number concentration and size of cloud droplets is in part set by the number concentration and properties of the aerosol (i.e., nuclei) that are present. More specifically, Twomey (1974) showed that an increasing aerosol number concentration with a fixed liquid water path increases the cloud droplet number concentration and decreases the cloud droplet size. This has been shown again and again in observational studies of all types, from satellite remote sensing, surface remote sensing, and in situ sampling (e.g., Twomey and Warner 1967; Warner and Twomey 1967; Kaufman and Nakajima 1993; Durkee et al. 2000; Feingold et al. 2003; Breon et al. 2002; Bert et al. 2011; Costantino and Breon 2013).

It is also agreed upon that smaller cloud droplets have lower collision efficiencies than larger droplets (Klett and Davis 1973) and therefore take longer to form warm rain through collision and coalescence (Lohmann and Feichter 2005; Khain et al. 2005). But whether this precipitation delay increases the total lifetime of a warm cloud as Albrecht (1989) suggested or decreases the total lifetime through convective invigoration and subsequent rainout as Stevens and Seifert (2008) suggested is undetermined.

What is clear from prior studies is that aerosol–cloud interactions extend beyond microphysics to dynamics and both must be considered together (Khain et al. 2005; Storer et al. 2010). In addition, the nature of aerosol–cloud interactions is highly dependent on various factors including the updraft strength within a cloud, the cloud type (warm, mixed, or ice phase), and location (latitude, over land or ocean) among many others; here we focus on aerosol–cloud interactions in tropical warm-phase orographic convective clouds.

b. *Aerosols in orographic scenarios*

Orographic clouds bring unique and valuable constraints to the study of aerosol–cloud interactions. The inclusion of mountains brings about a fixed forcing location and an imposed time constraint for convection. Mountains generally receive more rain than the surrounding area since an air mass that might otherwise be stable can become unstable from orographic lifting or elevated heating (Roe 2005). Because of the consistency of orographic forcing, a robust change in the precipitation caused by aerosol–cloud interactions can have significant impacts, especially when integrated over long temporal scales.

There is evidence for aerosol–cloud interactions in orographic clouds changing the spatial distribution of precipitation. A study by Muhlbauer and Lohmann (2008) looked at the spatial distribution of warm-phase orographic precipitation in highly idealized two-dimensional simulations in various dynamical flow regimes. They found that an increase in aerosol led to a downstream shift in orographic precipitation distribution and that the downslope precipitation enhancement depends critically on the width of the mountain and on the flow dynamics. Their simulations indicate that differences in latent heating induced by aerosol–cloud interactions can affect orographic dynamics and feedback onto the overall development of orographic precipitation.

There is also evidence for aerosol–cloud interactions in warm-phase orographic clouds changing the precipitation amount. A study by Lynn et al. (2007) obtained a 30% decrease of precipitation if aerosol conditions were changed from low to high aerosol number concentration to represent maritime and continental concentrations, respectively.

Other studies have looked at aerosol impacts on orographic cold and mixed-phase clouds (e.g., Xiao et al. 2014; Zubler et al. 2011) but here we undertake only warm-phase clouds and leave cold and mixed-phase clouds for future research.

This study focuses on the impact of aerosol–cloud interactions in orographic convection from a thermally driven perspective. Observations from the DOMEX field campaign suggest that warm-phase thermally driven orographic convection is sensitive to aerosol–cloud interactions from aerosols derived from the island surface (Smith et al. 2012; Nugent et al. 2014; Watson et al. 2015; Russotto et al. 2013). This relationship will be explored using an idealized numerical model with surface aerosol source differences. Section 2 describes the motivating DOMEX field campaign observations, section 3 provides the numerical model setup, the model results are summarized in section 4, a discussion of the results with respect to observations is included in section 5, and conclusions are covered in section 6.

2. DOMEX observations and studies

The DOMEX field campaign in April and May of 2011 observed the atmosphere with 21 research flights on fixed flight tracks around and over the complex terrain of an island called the Commonwealth of Dominica. Dominica lies in the Caribbean's Lesser Antilles at 15°N with a maximum elevation of 1.4 km (Fig. 1a). The University of Wyoming King Air aircraft was used to sample a range of low and high wind speed conditions, shallow trade wind convection, overisland convection, and the environmental air upstream and downstream of Dominica. Both microphysical and dynamical quantities

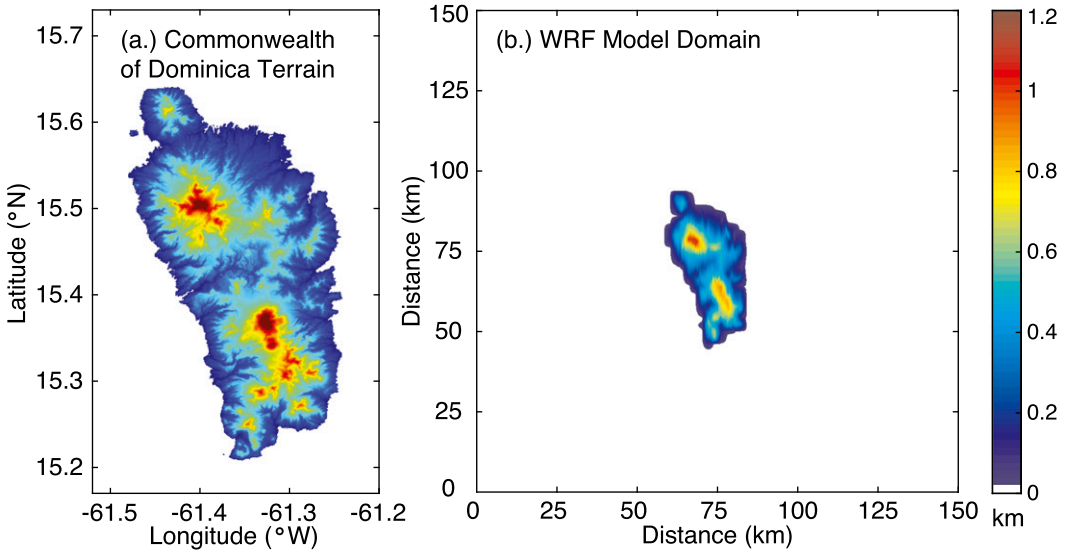

FIG. 1. Terrain elevation (color; km) for the Commonwealth of Dominica from (a) high-resolution SRTM and (b) the domain used for the WRF simulations with smoothed terrain. The entire WRF domain is 150 km × 150 km.

were measured. For more information on sampling strategies and flight tracks, see Smith et al. (2012).

Two orographic convective regimes dependent on wind speed were found during DOMEX (Smith et al. 2012). When the trade wind speed was weak ($<5\,\mathrm{m\,s^{-1}}$), thermal convection dominated over the island. The island surface temperature rose by 5°C, owing to surface heating and a lack of wind ventilation, while airflow divergence was found at a height of 1.8 km associated with cloud-top outflow near the height of the trade wind inversion (Smith et al. 2012; Nugent et al. 2014). When the trade wind speed was strong ($>8\,\mathrm{m\,s^{-1}}$), mechanically forced orographic convection was dominant. Low-level flow quickly approaching the island was forced to rise because of the terrain and became convective upon uplift (Smith et al. 2012; Nugent et al. 2014; Nugent and Smith 2014).

Connected with and forced by the trade wind speed changes are two atmospheric conditions that differed between the low and high wind speed convective regimes: (i) above-island aerosol concentration (Smith et al. 2012; Nugent et al. 2014) and (ii) upstream mid-tropospheric moisture (Watson et al. 2015). Differences were also seen in (iii) cloud microphysical properties and surface precipitation accumulation (Smith et al. 2012; Nugent et al. 2014) while (iv) physical cloud properties remained overall similar (Watson et al. 2015).

a. Aerosol concentration

Aerosol number concentration was measured in situ but out of cloud by aircraft with the passive cavity aerosol spectrometer probe (PCASP) in the diameter range from 0.1 to 3.0 μm (Cai et al. 2013). The aerosol concentration directly over Dominica at 1.8-km height is significantly higher during low wind speed conditions ($\sim 300\,\mathrm{cm^{-3}}$) as compared to high wind speed conditions ($\sim 100\,\mathrm{cm^{-3}}$). The elevated aerosol signal from two low-wind research flights (RF7 and RF8) is shown in Fig. 2a and 2b. Three consecutive "racetrack" shaped flight tracks show an aerosol "shroud" directly over Dominica that is distinct from the aerosol-free background flow to the north and south of the island. In the same region with elevated aerosol concentration, the CO_2 concentration is depleted (Figs. 2c,d), suggesting that the air has been in contact with the vegetated surface of Dominica and photosynthetic processes have taken place (Smith et al. 2012). It is hypothesized that when air comes in contact with the island surface, it gains heat, aerosol, and a reduced CO_2 concentration from the boundary layer and is buoyantly lofted above the island into the cloud layer (Smith et al. 2012; Nugent et al. 2014). The aerosol is not measured directly in cloud owing to limitations of aerosol measurement coincident with cloud measurement. Still, high aerosol concentration at cloud level outside of cloud can be accounted for by two mechanisms consistent with a surface aerosol source: (i) aerosols lofted in vertically moving air and (ii) detraining cloudy air that continuously adds aerosols that accumulate above the island.

During high wind speed conditions, the air measured over Dominica at 1.8-km height does not contain aerosol concentrations elevated above the background concentration nor depleted CO_2 concentration (not shown). When the wind speed is high, the boundary layer remains

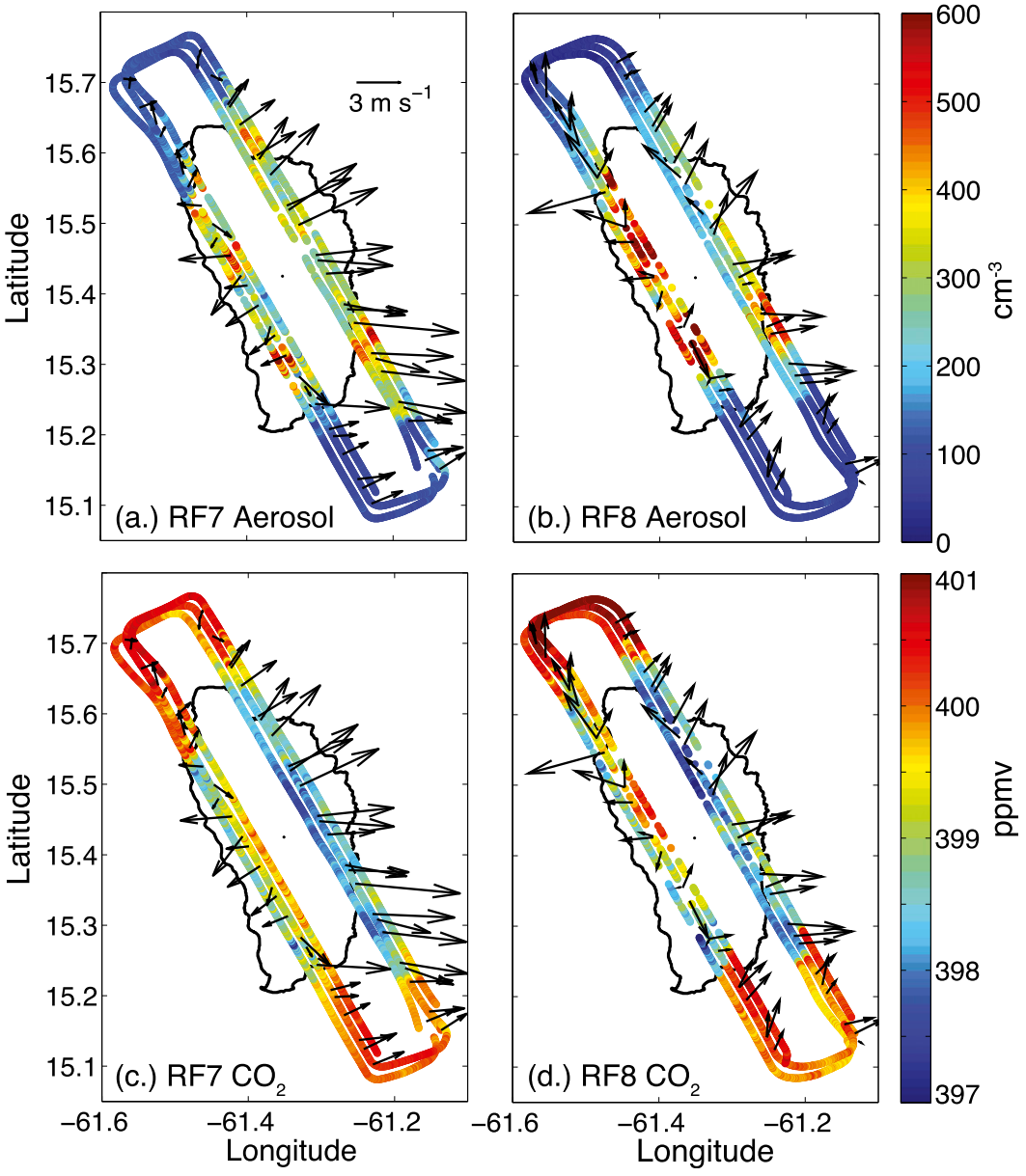

FIG. 2. (a),(b) Aerosol number concentration (color; cm^{-3}) and (c),(d) CO_2 concentration (color; ppmv) over Dominica (outlined in solid black) at 1.8-km height from 1-Hz in situ measurements on two low-wind research flights (RF7 and RF8). Three consecutive "racetrack" shaped identical flight tracks are slightly displaced for visualization purposes. When cloud is present, the aerosol and CO_2 concentrations are not displayed. We interpret the elevated aerosol and depleted CO_2 as a signature of the lofted and detrained air. Vectors indicate wind speed and direction.

shallow and any aerosol that may become mixed upward or detrained will be quickly carried downstream in the fast moving flow. This is shown in Nugent et al. (2014, their Fig. 15) where at high wind speeds, aerosols are transported downstream and do not accumulate over the island. A shallow CO_2 depleted island wake during high wind speeds is also seen in DOMEX aircraft observations measured at 300-m height ~20 km downwind of the island (not shown).

The role of wind speed for aerosol concentration is to control the depth of the boundary layer above the island. In classical formulations, the boundary layer depth d grows as $d = \mathrm{sqrt}(KL/U)$, where K, L, and U are the turbulent diffusivity, the distance downwind of the east coast, and the ambient wind speed. Air is well mixed within the boundary layer and is in direct contact with the island surface where it gains surface properties like elevated

aerosol concentration and heat. In strong winds, the boundary layer remains shallow and the aerosol and heat in the boundary layer are advected downwind and do not get caught up into the convection. In weak winds, the boundary layer grows quickly and hot aerosol rich air is drawn up into the convection above the island. In this way, the boundary layer depth controls the above-island aerosol concentration through wind speed.

Figure 3a shows aerosol concentration from both the PCASP instrument (0.1–3.0 μm) and the condensation nuclei counter (CN; 0.006–2.0 μm). The low and high wind aerosol transport mechanisms described result in changing aerosol concentration as wind speed changes. Both the PCASP and the CN counter instruments independently show a decreasing trend in above-island aerosol concentration with increasing trade wind speed from all 21 research flights. From these aerosol observations it is clear that if we want to study the impacts of aerosols on orographic clouds, we need to focus on the low-wind thermally driven days where aerosols are observed making it up to the cloud level.

b. *Midtropospheric moisture*

During low wind speed conditions, the midtropospheric cloud layer from ~1- to 2-km height was drier (RH = 60%) outside of cloud than during high wind speed conditions (RH = 85%) (Fig. 4a). This may be due to additional surface evaporation caused by higher latent heat fluxes from the ocean surface when the surface wind speed is high (Nuijens et al. 2009). The potential temperature profile (Fig. 4b) is similar during low and high wind speed conditions and differs by only a small shift of ~1 K. The cause for the minor shift in potential temperature involves virtual temperature and is discussed in Watson et al. (2015). Note that we use the term ''cloud layer'' throughout this document to mean the layer between the lifting condensation level of surface-based parcels (~600–800 m) and below the height of the trade wind inversion (~2–3 km). It is in this layer that trade wind cumuli normally form, though cloud coverage is generally small. The cloud-layer experiences considerably variable humidity from day to day.

c. *Cloud microphysics and precipitation*

In addition to the aerosol number concentration changes, observations of cloud droplets also differ with wind speed. Cloud droplets were measured in situ by the cloud droplet probe (CDP; 2–50 μm; Fig. 3b). Cloud droplet number concentration decreases with increasing wind speed and the cloud droplet diameter (Fig. 5) is smaller and more narrowly distributed during low as compared to high wind speed conditions. Less surface

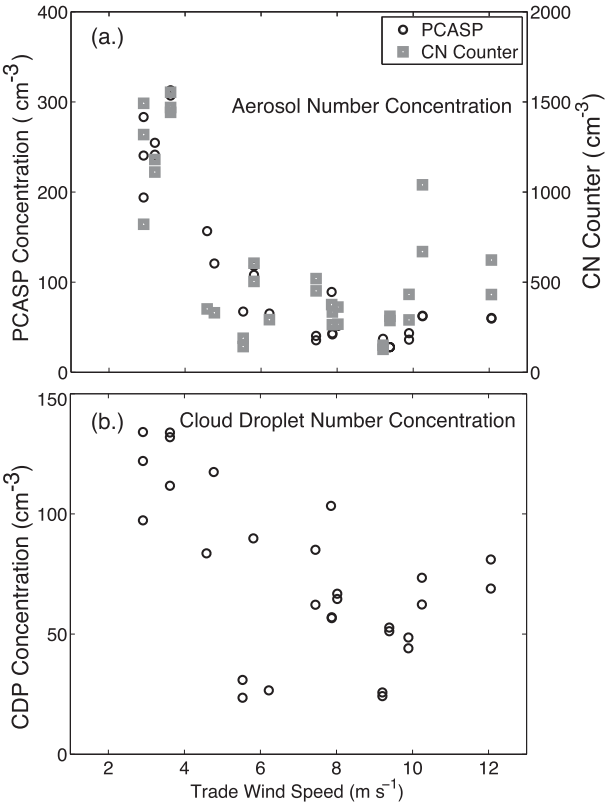

FIG. 3. (a) Average aerosol number concentration (cm^{-3}) measured by the PCASP and the CN counter instruments and (b) average cloud droplet number concentration (cm^{-3}) measured by the CDP instrument, all measured at 1.8-km height over Dominica and plotted against the average upstream wind speed ($m\,s^{-1}$, measured at 300-m height) for all research flights. Adapted from Smith et al. (2012).

precipitation is also observed on low-wind days when the cloud droplet size distribution is small and narrow. Figure 6 shows 24-h accumulated precipitation over Dominica as measured by the TFFR radar on Guadeloupe, an island just to the north of Dominica. The light precipitation in Fig. 6a looks mostly scattered and unrelated to the island while the heavy precipitation in Fig. 6b is centered over the terrain along the island spine (note the ×10 change in scale between Figs. 6a and 6b). For additional observational evidence of precipitation differences over Dominica on low and high wind days, see Smith et al. (2012) and Nugent et al. (2014). Included in Nugent et al. (2014) is a discussion about Dominica's lack of a diurnal cycle in precipitation, which is especially relevant here and helps us to conclude that the precipitation in Fig. 6a is not forced by Dominica.

Both (i) aerosol number concentration and (ii) midtropospheric moisture content can have an impact on cloud microphysics and precipitation (Grant and van den Heever 2014; Damiani et al. 2008; Parsons et al.

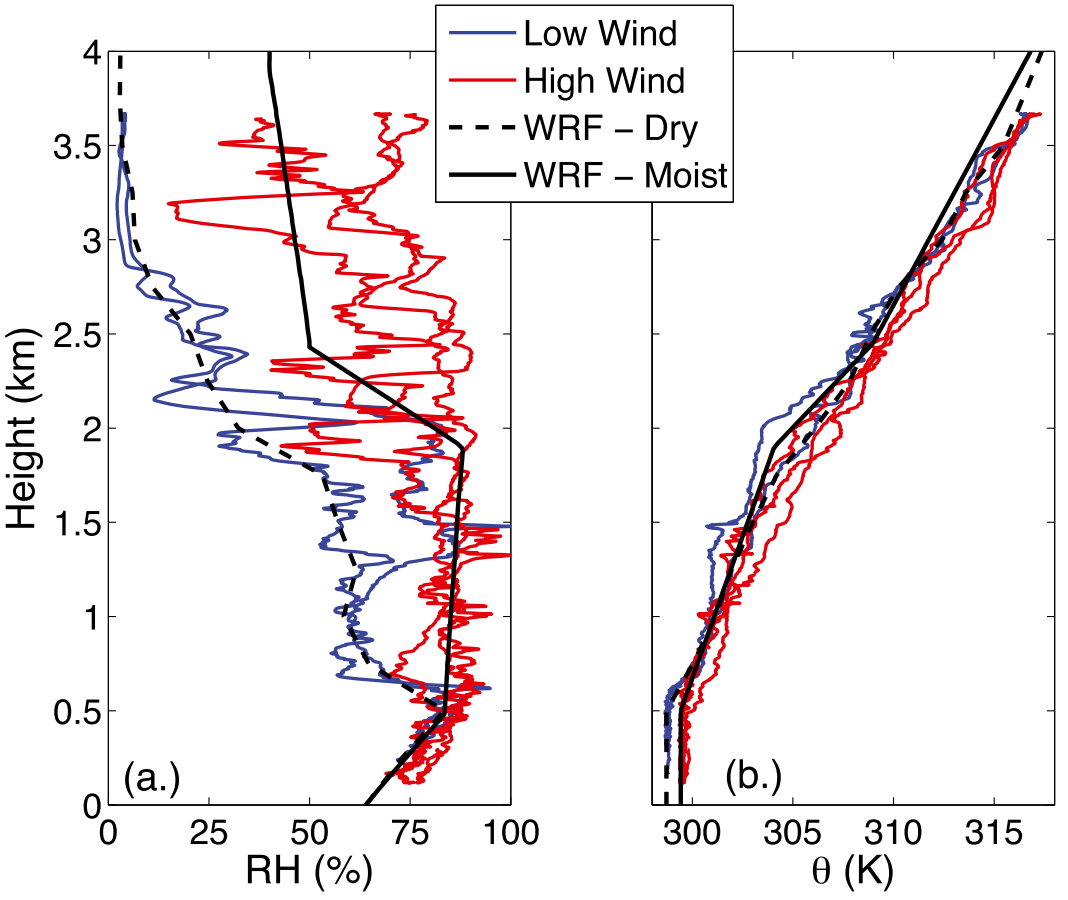

FIG. 4. Five aircraft measured soundings during high wind speed periods (red: RF13, RF17, and RF18) and low wind speed periods (blue: RF7 and RF8). (a) Relative humidity (RH; %) and (b) potential temperature (θ; K) are shown from observations in addition to the solid (dashed) black lines, which show the potential temperature and humidity used for the initiation of the moist (dry) WRF simulations.

2000; Mapes and Zuidema 1996; Fan et al. 2007; Ackerman et al. 2004). Cloud observations in Figs. 3b and 5 are consistent with theory described in section 1 and smaller more numerous cloud droplets are less efficient at colliding and coalescing to form precipitation sized drops, therefore reducing precipitation efficiency (Rosenfeld 1999; Lohmann and Feichter 2005). A dry cloud layer can also inhibit vertical growth of clouds (Stevens 2005; Damiani et al. 2008; Zehnder et al. 2009), which can account for a decreased cloud droplet size and a reduction in precipitation. However, a dry cloud layer cannot account for an increased cloud droplet number concentration.

d. *Physical cloud properties*

An extensive cloud scale study of the observed cloud dynamical properties on low and high wind days was undertaken in Watson et al. (2015). They found that the physical characteristics of the orographic clouds on low and high wind days were similar in their distribution of vertical velocity and liquid water content. However, low-wind days often had shallower cloud-top heights, and Watson et al. (2015) found that the impact of entraining dry air into cloud could account for this cloud-top height difference.

e. *The complexity of understanding DOMEX precipitation*

The DOMEX field campaign was initially designed to observe the typical conditions over the island of Dominica: mechanically forced orographic convection and precipitation under medium to strong trade wind flow. Medium to strong trade wind flow was only observed during DOMEX approximately half of the time. The other half of the time during DOMEX observed a climatologically rare state of weak trade winds (20% of the time climatologically) and a relatively dry mid troposphere (16% of the time climatologically), which occur even less frequently in tandem [climatological statistics from Watson et al. (2015)]. The recurring difficulty

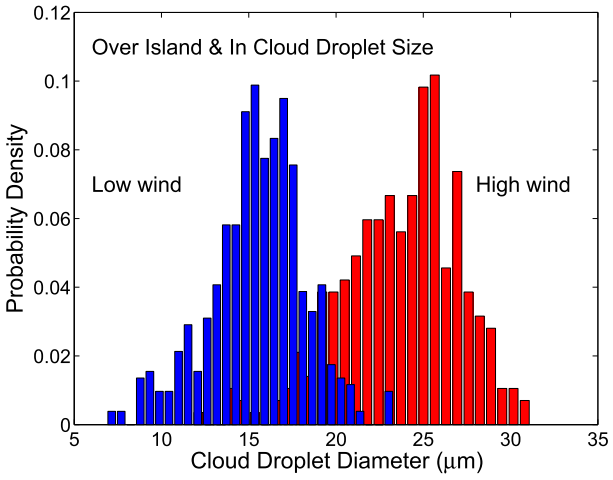

FIG. 5. Overisland cloud droplet diameter (μm) measured at 1.8 km under low (RF7) and high (RF13) trade wind conditions during DOMEX. Note the difference in mean diameter and the distribution spread. Adapted from Smith et al. (2012).

of understanding the controls on precipitation over Dominica are described below.

A mainly observational study by Watson et al. (2015) focused on understanding the processes controlling precipitation with regards to (i) convective triggering mechanisms, (ii) dry-air entrainment, and (iii) giant sea-salt aerosol. After thorough observational and numerical comparison of low, medium, and strong wind days they concluded that the complex interplay of the three processes make determining a single controlling mechanism for precipitation difficult yet (ii) and (iii) remained the most plausible. The role of island-derived aerosol was not considered in Watson et al. (2015).

Another recent study by Wang and Kirshbaum (2015) used the Weather Research and Forecasting Model to study Dominica's thermal circulations on low-wind days and on the topic of precipitation they conclude that rain suppression could be caused by (i) entrainment of dry cloud-layer air, (ii) detachment of the cloud tops from the cloud bases, or (iii) high aerosol concentration. Wang and Kirshbaum (2015) compare model simulations and sensitivities to many parameters including grid resolution, cloud shading, boundary layer winds, and topographical forcing yet all simulations produced much larger ($\times$20) rainfall maximas than observed. Their cloud droplet number concentration was fixed at 200 cm^{-3}, with one sensitivity test of 300 cm^{-3}, but the role of small island-derived aerosols was not considered.

Understanding the sharp reduction in precipitation observed on low-wind days over Dominica remains one of the biggest unknowns in DOMEX. The physical characteristics of the convection (i.e., cloud liquid water contents and vertical velocities) under both low and high wind conditions are surprisingly similar (Watson et al. 2015) and yet low-wind days hardly precipitate (Smith et al. 2012; Nugent et al. 2014). Here we focus on understanding the role of accumulation mode aerosols from a surface source in low-wind thermally driven convection and the development of precipitation. We hypothesize that aerosols lofted into the convection can account for the observed microphysics and the precipitation reduction.

We take a model-driven approach and have two main goals. First, we want to understand how aerosols affect thermally driven orographic convection and the development of warm rain and how those effects are sensitive to cloud-layer moisture and the presence of a background wind. We start with the simplest case possible

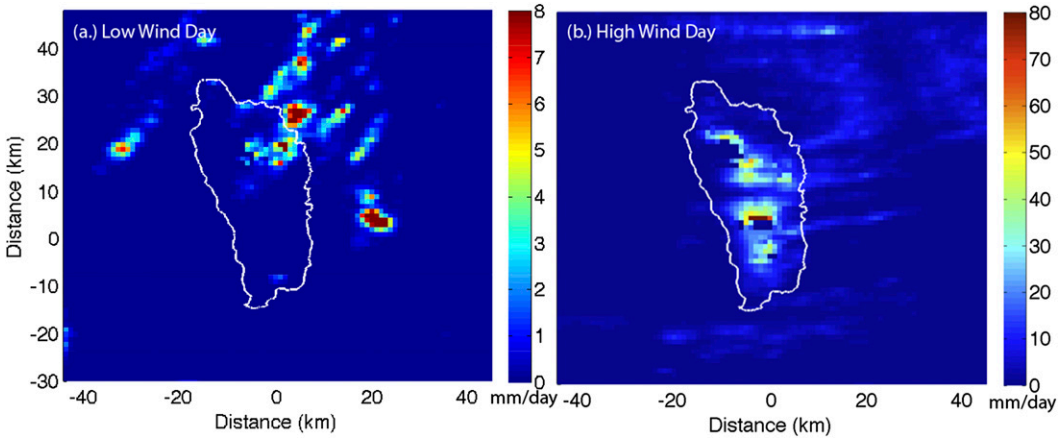

FIG. 6. Twenty-four-hour rainfall accumulation (mm day^{-1}) for a (a) low-wind day (RF7) and a (b) high-wind day (RF13) from the Météo-France Guadeloupe TFFR radar. Note the $\times$10 difference in scale between (a) and (b) and the minor beam blockage from terrain that remains uncorrected.

and build complexity. Second, we want to directly compare observations with the model to test our hypotheses and gain further insight.

3. Numerical model setup

Numerical simulations were performed using the Weather Research and Forecasting (WRF) Model (Skamarock et al. 2008) version 3.6.1. WRF is a fully compressible nonhydrostatic model on a mass-based terrain-following grid. A 200-m grid spacing is used to capture convective scale features, within the range suggested by Wang and Kirshbaum (2015) for this case. The vertical grid spacing is slowly stretched from 29 m near the surface to 500 m at the model top at 20 km with 99 vertical levels. A 1-s time step with 5-min output is used for a total time length of 12 h.

We use a smoothed "Dominica-like" terrain centered in a 150-km square domain (Fig. 1b). A sinusoidal varying surface sensible heat flux (SHF) is added over the terrain beginning at 0 $W m^{-2}$ at time 0, the equivalent of 0600 local time, when the simulations begin, increasing to $SHF_{max} = 200\ W m^{-2}$ at hour 6 (1200) and decreasing again to 0 $W m^{-2}$ at hour 12 (1800) when the simulations end. We include no SHF over the ocean and no latent heat flux over the terrain or over the ocean. Neither radiation nor PBL parameterizations are used.

A simple cloud shading technique has been included to parameterize the impacts of cloud shading on the SHF over the mountain, suggested as an important parameter in surface heating by Nugent et al. (2014) and Wang and Kirshbaum (2015). We assume a zenith sun angle where the cloud liquid water content (LWC) impacts the sinusoidally varying SHF in the following way:

$$\mathrm{SHF} = \mathrm{SHF}_{\max} \times \sin\left(\frac{\pi t}{t_{\mathrm{end}}}\right) \times \exp\left(\frac{-\mathrm{LWC}}{\mathrm{LWC}_{\mathrm{ref}}}\right), \quad (1)$$

where t indicates time, $t_{end} = 12$ h, and LWC_{ref} was chosen to be 1 $g m^{-3}$. This technique effectively reduces the SHF in locations where clouds lie directly overhead. When the column integrated LWC exceeds 1 $g m^{-3}$, the SHF reduces nearly to zero. This shading, together with the complex terrain and (when present) ambient wind, randomizes the convection and prevents a single large plume from forming over the island.

Idealized soundings (black solid and dashed lines in Fig. 4) were used to initialize the model simulations [solid "WRF-moist" is identical to the sounding used by Minder et al. (2013)]. Below 4 km, the temperature and moisture fields in the idealized soundings were designed to match high- and low-wind DOMEX aircraft soundings while the atmosphere above 4 km has uniform stratification. Both soundings are conditionally unstable. Note that as visible in Fig. 4a "WRF-dry" is not a completely dry sounding, but just relatively dry as compared to the "WRF-moist" sounding. The notation "dry" with reference to the atmospheric profile throughout this document is used consistently in this manner. Additionally, two constant-with-height wind conditions are tested, 0 and 2 $m s^{-1}$, and in both, thermally driven circulations develop with time as a result of the surface sensible heating.

A 1.5-order TKE closure scheme was used along with a monotonic sixth-order filter to damp grid-scale variability (Knievel et al. 2007). Periodic lateral boundary conditions are used, though open boundary conditions provided nearly identical results. Time stepping was done with a third-order Runge–Kutta method, while advection used fifth-order horizontal and third-order vertical methods. A sponge layer above 12-km altitude damps vertical velocities to avoid unrealistic reflection off the model top (Klemp et al. 2008).

The Thompson microphysics scheme with coupled aerosol–microphysics is used (Thompson and Eidhammer 2014). The scheme is two moment for cloud and rainwater and includes predictive aerosol variables for CCN and ice nuclei (IN). An aerosol concentration probability density function around a user chosen mean is used to predict explicitly the cloud droplet number concentration based on a lookup table of activated fraction determined by the model's temperature, vertical velocity, number of available aerosols, hygroscopicity, and aerosol mean radius. The strongest dependence in the scheme is on the vertical velocity and the number of available aerosols. No ice-phase microphysics are considered in this study as the clouds do not extend above the 0°C level.

Aerosols are coupled and interactive with the model microphysics including sources of aerosols from evaporating cloud droplets and raindrops and surface emissions and sinks by activation as CCN and scavenging by precipitation. The initial aerosol background characteristics in all simulations have a mean size of 0.16 μm and 0.6 hygroscopicity with a near surface concentration of 300 cm^{-3}, which decreases exponentially with height to a constant value of 50 cm^{-3} beginning around 3 km. In simulations with an aerosol source (AS), a surface aerosol source is imposed for the over mountain regions only where the elevation exceeds 5 m. The source quantity is 5 aerosols $cm^{-3} s^{-1}$, which is equivalent to a surface flux of 1.45×10^8 aerosols $m^{-2} s^{-1}$ spread over the lowest model level depth of 29 m. An aerosol surface source on Dominica has not been observed, and instead the model source quantity was chosen through trial and error as the lowest possible source value that compared well with

in situ observations at aircraft level (1.8 km). In simulations with no aerosol source (NS), only a small surface aerosol source of 1 aerosol $cm^{-3} s^{-1}$ is imposed (2.9×10^7 aerosols $m^{-2} s^{-1}$), designed not to increase surface aerosol concentrations, but to keep aerosol concentrations from becoming unrealistically depleted.

Three sets of simulations are performed, six simulations in total (Table 1) to explore the influence of aerosol source quantity, atmospheric moisture content, and wind speed. The motivation for this simulation set is described in section 4.

TABLE 1. The names and parameters used for the three simulation sets. Background wind speed, AS and NS for simulations with (aerosol source) and without (no source) a significant surface aerosol source over the island area, and dry or moist to specify whether the atmospheric profile has a relatively dry or moist cloud layer are included. Note that dry does not imply no moisture, but simply relatively low moisture.

Group name	Wind speed ($m s^{-1}$)	Aerosol	Moisture
Set 1	0	AS and NS	Dry
Set 2	2	AS and NS	Dry
Set 3	2	AS and NS	Moist

4. The changing aerosol impact as wind and humidity vary

Numerical simulations are performed to gain insight into the role of a surface aerosol source in orographic convection. We begin in section 4a with Set 1, the simplest thermally driven orographic scenario with no background wind and a heated surface. Additional attention is given to the domain total water and aerosol budget in this simple case to build confidence and understanding in the model results. Later in sections 4b and 4c a weak background wind and moisture are added in succession in Sets 2 and 3.

To understand how aerosols are impacting the development of precipitation, the simulations are analyzed in a bulk sense. This allows an understanding of how the convective system behaves as a whole. Later in section 5 the simulations are compared directly to DOMEX observations.

a. Set 1: Dry sounding and 0 m s^{-1} wind

First we consider the simplest case of thermally driven orographic convection where no background wind is imposed on the domain. We call this Set 1 and the relatively dry sounding with two aerosol states are tested: with an AS and with effectively NS as seen in Figs. 7a and 7b after 6 h. Because of the sinusoidally varying surface heat flux, a thermally driven circulation develops with time. As the circulation develops, air rises up both sides of the mountain and converges at the mountain top. Heating and surface convergence drive vertical motion creating convective clouds over the mountain. As the convection continues to develop, aerosols are lofted, clouds grow vertically, and precipitation begins to form. Because there is no background wind, the convective system is symmetric and precipitation that forms falls directly onto the clouds forming below. At cloud top in the AS case, aerosol laden air diverges and spreads horizontally away from the island creating an aerosol shroud, similar to the observed aerosol shroud from Figs. 1a and 1b.

A domain integrated water budget is easily constructed. As convection develops, water vapor is depleted from the domain by condensation and subsequent storage in the form of cloud and rainwater. The summation of the instantaneous cloud water (QC) and rainwater (QR) in the atmosphere, in addition to the integrated surface precipitation (PR) is equivalent to the amount of water vapor depleted from the domain:

$$\mathrm{QV}_{\mathrm{init}} - \mathrm{QV}(t) = \mathrm{QC}(t) + \mathrm{QR}(t) + \int_0^t \mathrm{PR}(t)\, dt, \qquad (2)$$

where QV(t) indicates instantaneous domain integrated water vapor at time t, and $\mathrm{QV}_{\mathrm{init}}$ is the domain integrated water vapor at the beginning of the simulation. Figure 8a shows the domain total evolution of how these quantities develop in a bulk sense in both Set 1 simulations throughout the 12-h duration. The water budgets do not close completely because of unrecorded 1-s time steps between the 5-min output interval, but only 3.7%–6.2% of the depleted water vapor remains unaccounted for. By the end of the simulation, Set 1 NS loses ~8% more QV from the domain (i.e., precipitates 8% more) than the Set 1 AS simulation (Figs. 8a and 9a).

In Figs. 8 and 9, we emphasize budgets. For cumulative surface precipitation (Figs. 9a–c), this means that the units are given in kilograms to compare with kilograms of liquid water in the atmosphere, not millimeters as is customary. One can convert from kilograms to millimeters easily by dividing by the density of water and the island area (865 km^2 in the model, slightly larger than the actual island area because of smoothing) and converting to the desired units.

The temporal evolutions of QC and QR are shown in Fig. 9d along with a scaled SHF curve for reference. The initial conditions of the Set 1 pair are the same except for the surface aerosol source. QC develops identically in both Set 1 simulations until hour 4 when QR develops first in the Set 1 NS simulation, driving differences in QC that are small at first and grow larger with time. The heavier precipitation in Set 1 NS than Set 1 AS at hour 6

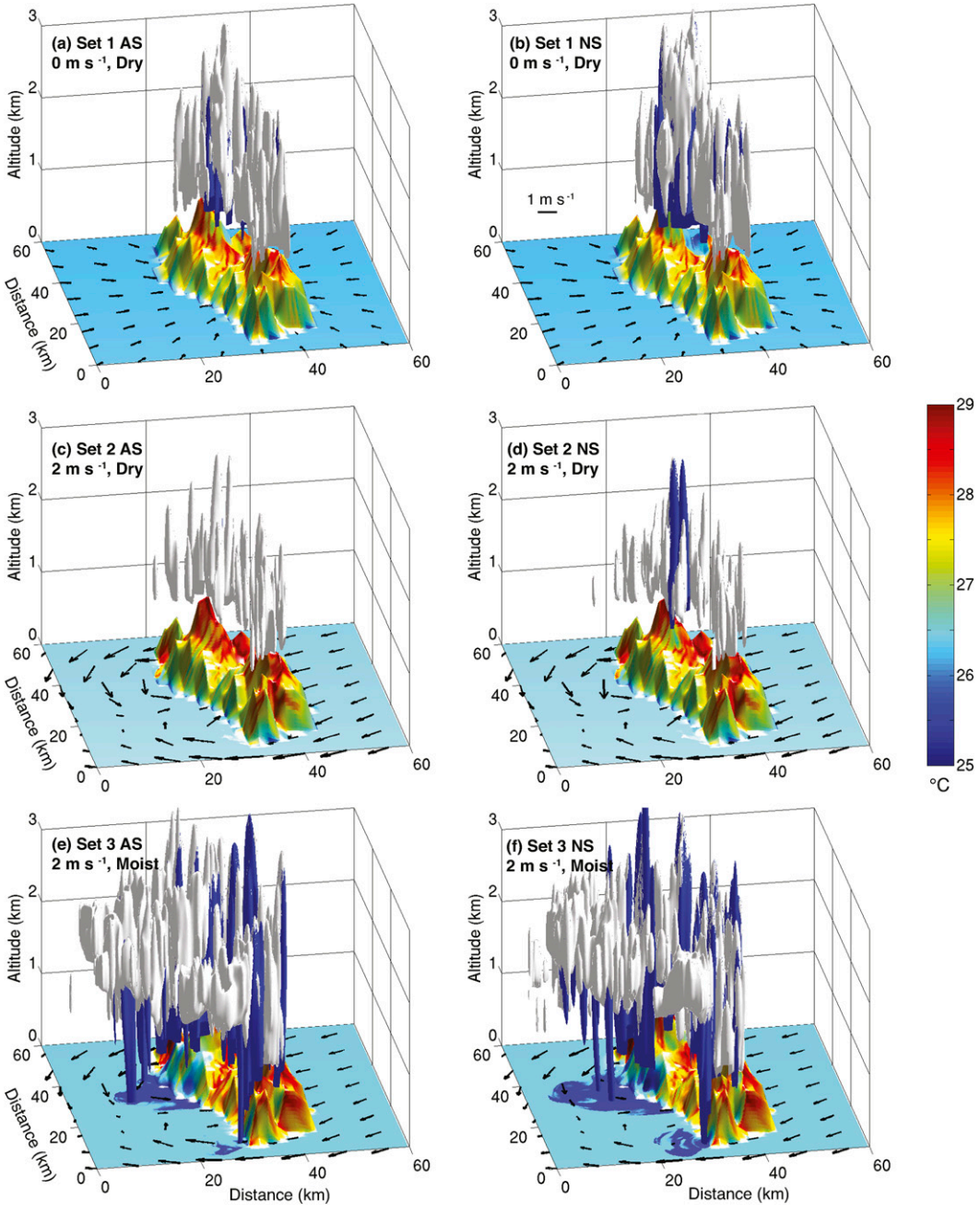

FIG. 7. A sample image of the 3D domain for each model run at 6 h into the simulation time with isosurfaces of cloud liquid water content (white) and rainwater content (blue; both at 0.1 g kg^{-1}). The surface color indicates the potential temperature (°C) at the lowest model level and wind vectors indicate wind speed and direction at the lowest model level with a reference vector in (b). (a) Set 1 AS, (b) Set 1 NS, (c) Set 2 AS, (d) Set 2 NS, (e) Set 3 AS, and (f) Set 3 NS as viewed from the south-southwest looking north-northeast. Note that only a subsection of the domain is shown.

is easily visualized in Fig. 7b versus Fig. 7a. Overall more liquid water in the Set 1 AS simulation is stored in QC than QR (Fig. 9d). The peak of QR is displaced less than 1 h from the time of SHF_{max} (hour 6) in Set 1 NS while AS lags in time with a peak in QR not until 2.5 h after SHF_{max}. The higher cloud water storage in Set 1 AS acts as a buffer and allows it to approach a similar total precipitation amount as Set 1 NS at later times.

The initial differences in the Set 1 pair are driven by microphysical processes as the only differing factor is the surface aerosol source. However, microphysical and dynamical processes need to be considered together

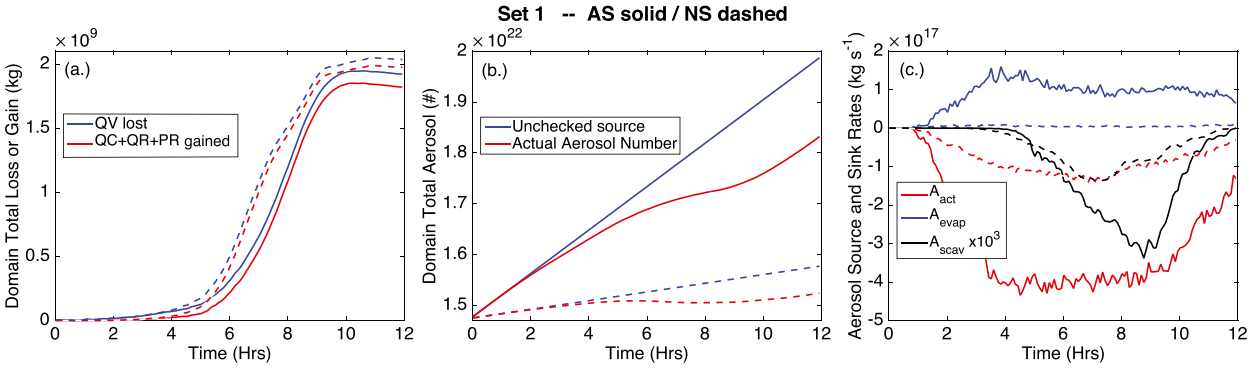

FIG. 8. Domain total evolution of (a) water vapor (QV; blue) lost from the domain and liquid water (QC + QR + PR; red) gained in the domain as given in (2), (b) aerosol number concentration as it would evolve without sinks (blue) and as it does evolve (red), and (c) the source and sink terms (activation A_{act}, evaporation A_{evap}, and rain scavenging A_{scav}) accounting for changes in domain total aerosol number concentration in the Set 1 AS (solid) and Set 1 NS (dashed) simulations.

(Khain et al. 2005) since dynamical differences can develop from temporal changes in both phase changes of water and precipitation formation. The domain maximum and minimum vertical velocity (left axis) through time as well as the cloud-top height (right axis) is shown in Fig. 9g. The dynamics of Set 1 simulations have only slight differences and there is evidence for convective conditioning of the atmosphere [as in Zehnder et al. (2009)] as cloud-top heights continuously grow higher and higher, even as the solar heating decreases (Fig. 9g). The above-island air moistens and becomes "conditioned" for deeper convection.

Microphysical differences between the Set 1 pair are investigated in Fig. 8b with the domain total aerosol number. The blue lines show the total number of aerosols in the domain assuming an unchecked surface aerosol source with no sinks. Recall that the aerosol surface source on Dominica was not measured but was set in the model by trial and error to match observations at aircraft level. The red curve in Fig. 8b shows the actual domain total aerosol number. For the Set 1 NS simulation (dashed red), the actual aerosol number stays approximately constant, as designed. More can be learned by looking into the aerosol budget to see what happens to the aerosol over time. Questions like "How many aerosols accumulate in the domain?" or "What is the largest sink of aerosols?" can be easily answered.

The total number of aerosols in the entire domain of the Set 1 pair is 1.47×10^{22} at startup. After 12 h, with the aerosol surface source of 5 (1) aerosols cm^{-3} in the Set 1 AS (NS) simulation, 1.8×10^{22} (1.5×10^{22}) are left, a gain of 25% (3%). Aerosols are added into the domain every second only over the terrain, a total area of 865 km^2. The surface aerosol source is distributed over the height of the lowest grid box (29 m) yielding a surface flux of 1.45×10^{8} (2.9×10^{7}) $m^{-2} s^{-1}$ or 1.25×10^{17} (2.51×10^{16}) aerosols added every second in the Set 1 AS (NS) simulation. After 12 h, a total of 5.42×10^{21} (1.08×10^{21}) aerosols are added into the domain.

The aerosol source and sink terms (excluding the surface source) are shown in Fig. 8c. The variables include a source of aerosol from evaporating cloud droplets (A_{evap}), aerosol depletion by activation as cloud droplets (A_{act}), and aerosol depletion by rain scavenging (A_{scav}, $\times 1000$). Evaporation is largely controlled by dry air entraining into the cloud. It causes a shroud of detrained aerosol (as in Figs. 2a and 2b). Overall the largest sink for aerosol number concentration is through A_{act}. A complete aerosol budget is impossible since aerosol combination in cloud and raindrop(let)s readily occurs and aerosols are not tracked after activation.

In addition to tracking the sources and sinks of aerosols through time, their impact on cloud and rain number concentration, cloud droplet diameter, and precipitation formation can be computed. An average over the time of peak convection (hours 6–10) yields a 256% increase in domain total cloud droplets in the Set 1 AS simulation as compared to NS and a 63% decrease in the number of raindrops (Table 2). A decrease in raindrop number with increasing aerosol was also found by Saleeby et al. (2015). Accompanying this change in cloud and rain number concentration comes a 38% decrease in the domain average mean volume diameter (MVD) of cloud droplets from 21.7 μm in the Set 1 NS simulation to 13.4 μm in Set 1 AS (Table 2). These cloud microphysical changes have a modest impact on precipitation formation by delaying precipitation in the Set 1 AS simulation as compared to NS (Fig. 9a).

The precipitation delay can be understood through two warm rain processes: autoconversion and accretion. Autoconversion is the numerical term for collision and coalescence and is the first step in precipitation formation

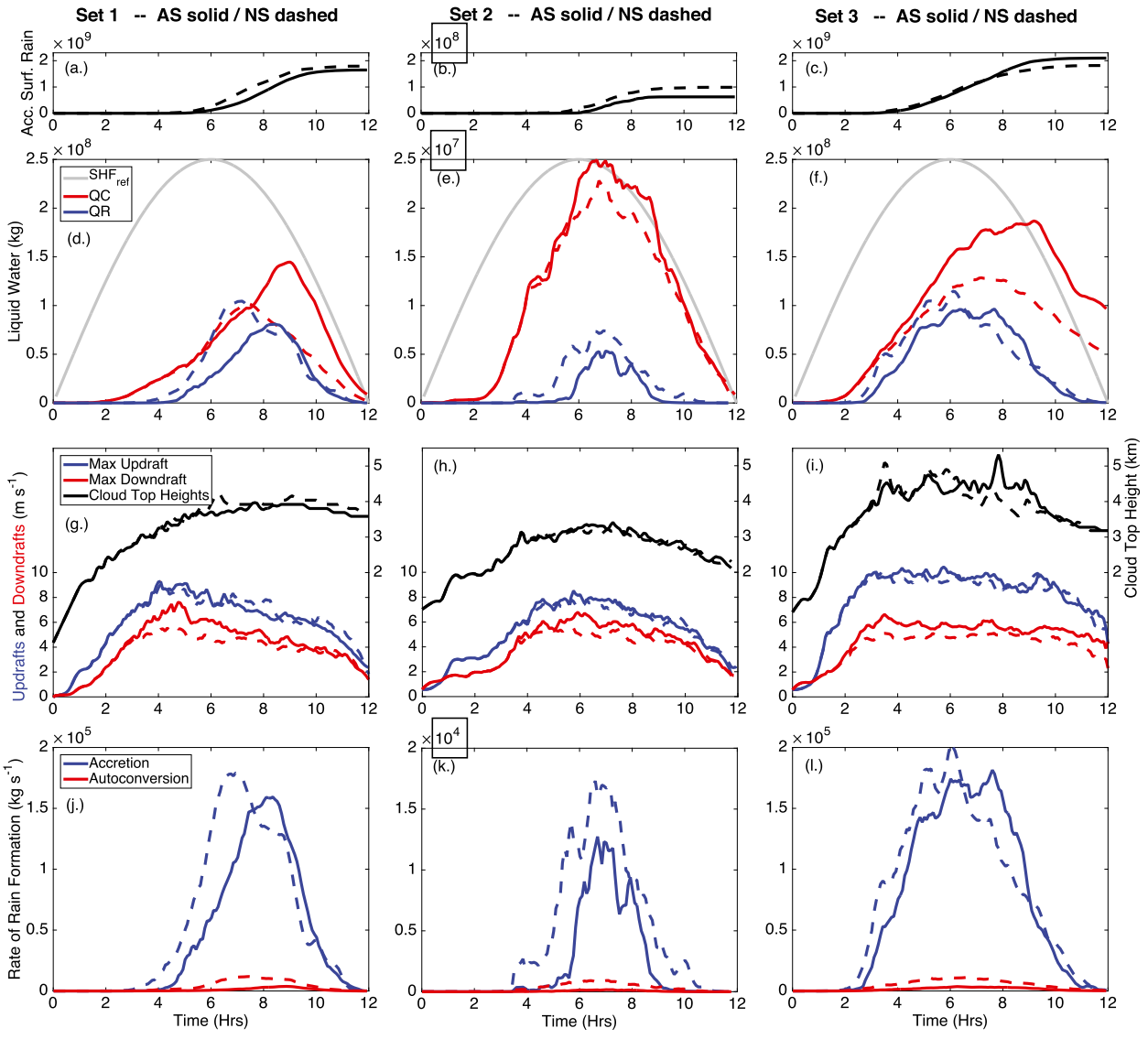

FIG. 9. Domain total evolution of (a)–(c) cumulative surface precipitation (kg), (d)–(f) cloud (QC; red) and rain (QR; blue) liquid water (kg) with SHF_{ref} displayed in gray as a timing reference, (g)–(i) maximum updraft (blue) and downdraft (red) velocities (left; m s^{-1}) and cloud-top heights (black, right; km), and (j)–(l) rate of rain formation (kg s^{-1}) through accretion (blue) and autoconversion (red) for all three sets of simulations as labeled along the top with AS (solid) and NS (dashed) simulations displayed for each set. Note the ×10 smaller change in *y*-axis scale for Set 2 simulations, boxed for emphasis in (b),(e), and (k).

whereby cloud droplets collide and combine to form larger and larger droplets that can begin to fall as rain. Next, accretion occurs whereby falling raindrops collect smaller cloud and raindrop(let)s. There is no fixed autoconversion threshold in the Thompson microphysics scheme, but rain generally begins to form when the cloud MVD exceeds 15 μm. Again, there is no fixed threshold, but the Thompson rain category begins around a "drizzle" drop size of about 50 μm and hence accretion begins when both rain and cloud water are present. The rate of rain formation through autoconversion and accretion is shown in Fig. 9j. The magnitude of the accretion rate in both Set 1 simulations is similar, but again precipitation formation in Set 1 AS is delayed. Autoconversion rates here, and in general, are significantly smaller than accretion rates though autoconversion in Set 1 NS is noticeably larger than Set 1 AS. To compare the magnitude of accretion and autoconversion, their ratio during the time of initial precipitation formation (hours 4 to 6) is included on the right side of Table 2. The accretion to autoconversion ratio is 83 in the Set 1 AS simulation and 24 in NS, meaning that the rate of rain formation through accretion is 83(24) times more active than the rate of rain formation through autoconversion in the Set 1 AS(NS)

TABLE 2. (left) The percent change from the NS to AS simulations for cloud number concentration, rain number concentration, MVD, and simulation total precipitation calculated as the average over the time of peak convection from hours 6–10. (right) The ratio of rain formation through accretion to autoconversion as precipitation is developing from hours 4–6 in each simulation.

	NS to AS change (%)				Accretion/autoconversion ratio	
	Cloud number	Rain number	MVD	Precipitation	AS	NS
Set 1	256	−63	−38	−8	83	24
Set 2	207	−67	−29	−37	26	12
Set 3	260	−34	−38	16	58	17

simulation. A larger ratio of accretion to autoconversion with a larger surface aerosol source shows the decreased efficiency of autoconversion in clouds with many small droplets.

The accretion to autoconversion ratios are the largest out of any set in the Set 1 pair (Table 2) owing to the symmetry of the convective system with no background wind, which strongly favors accretion. While thermally driven convection with no background wind is a useful way to begin to understand basic phenomenon, in nature, a no-background wind scenario is extremely unlikely so we turn to a weak background wind reminiscent of the low-wind conditions on days with thermally driven conditions. This helps to approach realism, avoid storm symmetry, and avoid overdominant accretion. We begin in section 4b with an identical setup to Set 1 but use a constant-with-height $2\,\mathrm{m\,s^{-1}}$ wind. We call this simulation pair Set 2.

b. *Set 2: Dry sounding and $2\,m\,s^{-1}$ wind*

By increasing the background wind from 0 to $2\,\mathrm{m\,s^{-1}}$, we anticipate three changes in the clouds over Dominica. First, the wind will ventilate the island surface and carry heat away, reducing the convective forcing. Second, the wind will carry clouds to the west, reducing the potential for cloud droplet scavenging (accretion). Third, the wind will refresh the region above the island with environmental air, carrying away any detrained cloud moisture. As the width of Dominica is only 20 km, the residence time of air over the island for a $2\,\mathrm{m\,s^{-1}}$ wind is only 2 h so the wind is significant. We do not test higher wind speeds to avoid the transition from thermally driven convection to mechanically forced convection that begins around $5\,\mathrm{m\,s^{-1}}$ (Nugent et al. 2014).

Initially the changes in the Set 2 simulations with a weak wind speed seem minor. Instead of air converging over the mountain peaks, air converges just to the lee side of the island crest (not shown). Cloud liquid water forms an hour sooner than in Set 1, driven by the additional weak wind forcing; the atmosphere still takes time to heat, but instead of the heating solely driving the circulation, a weak wind speed gives the airflow a moving head start. Still, the thermal forcing controls the convection and it strengthens and weakens with the sinusoidal surface heat flux over the 12-h simulation duration (see QC in Fig. 9e). The cloud-top heights in Set 2 are shallower than Set 1 and the up- and downdrafts are weaker, though they are remarkably similar among the Set 2 pair (Figs. 7c,d and 9h). The peak precipitation forms just after the peak heating (Figs. 9b,e). Interestingly, Figs. 7c and 7d capture Set 2 right at the time of peak heating, and Set 2 NS is clearly raining while Set 2 AS is not.

Perhaps the most remarkable difference between Set 1 and 2 is that with wind, less than 1/10th of the total accumulated precipitation from Set 1 forms in Set 2 (Fig. 9a vs Fig. 9b; note the ×10 decrease in scale). Also, little difference in timing and only small differences in magnitude are found in the Set 2 cloud and rain liquid water contents (Fig. 9e). Comparing Set 2 to Set 1, more liquid water is stored in cloud as compared to rainwater (Fig. 9e vs Fig. 9d) because of the smaller amount of rain production in Set 2, which maintains liquid water in the cloud phase. Overall, the total amount of cloud water, rainwater, and surface accumulated precipitation in Set 2 is significantly less than in Set 1.

The time average domain total cloud droplet number concentration during peak convection yields a 207% increase in the Set 2 AS simulation as compared to NS and a 67% decrease in the number of raindrops (Table 2). MVD drops from 17.8 to 12.7 μm, a 29% reduction (Table 2). Precipitation formation in Set 2 is not shifted in time as it is in Set 1; Set 2 NS produces precipitation first, but also produces precipitation for a longer duration than Set 2 AS (Figs. 9e,k). The rate of accretion again dominates in Set 2 simulations, though the accretion to autoconversion ratio decreases to 26 and 12 in the Set 2 AS and NS simulations (Table 2). This is not because autoconversion is more efficient in Set 2 than in Set 1 simulations but because of the overall reduction in precipitation.

c. *Set 3: Moist sounding and $2\,m\,s^{-1}$ wind*

In Set 3 we test the role of the cloud-layer moisture. The simulations are otherwise identical to Set 2. A weak wind day with a moist cloud layer was not observed during DOMEX, but this combination completes the set of possibilities for comparing aerosol effects and cloud-layer moisture effects on thermally driven orographic convection. A high wind day is not examined as convection on high wind days is orographically, not thermally

forced, and because aerosols are both (i) not lofted and (ii) quickly swept downstream in the fast moving flow.

By increasing the cloud-layer moisture (from the WRF-dry sounding to the WRF-moist sounding in Fig. 4) we anticipate two major changes in the convection. First, any clouds that form will ascend into air with a higher water vapor content. This means that the process of dry-air entrainment will be less effective. With less effective entrainment, clouds can maintain their moisture and buoyancy for a longer duration. Second, even though the $2\,m\,s^{-1}$ wind will refresh the above-island air, it will refresh it with relatively moist air. This means a continuous source of moisture for the convection, a larger water vapor flux, and a higher potential for precipitation.

Dynamically, the Set 3 simulations begin just as Set 2 began. Driven by the surface heating and a weak wind, air converges just to the lee of the island crest, with early cloud water formation and a moving head start from the weak wind. However, Set 3 evolves more rapidly than Sets 1 and 2 and updraft strengths and cloud-top heights quickly grow (Fig. 9i). This is easily seen in Fig. 7 where all simulation images are from hour 6, but Set 3 is precipitating heavily while Sets 1 and 2 are not. Differences between the Set 3 AS and NS simulations also rapidly grow as precipitation begins to form after 3 h instead of 5 or 6 h as with Sets 1 and 2 (Figs. 9c,f). Accumulative precipitation in Set 3 simulations exceeds Sets 1 and 2 (Fig. 9c). After the surface heating begins to weaken, rainwater decreases but cloud liquid water continues to grow and substantial cloud liquid water exists for the remainder of the simulation (Fig. 9f). By the end of the simulation, much of the cloud liquid water that is left exists as an elevated layer downstream of the island (not shown).

The stronger convective system in Set 3 with a moist cloud layer was expected, but it also held some surprises. For the first time, the AS simulation precipitates more than NS (Fig. 9c, Table 2). This will be further discussed in section 6.

The Set 3 cloud liquid water in the domain is the largest out of all sets and lasts longer than Set 1 or 2, even after heating has decreased (Fig. 9f). Comparable with Set 1 and 2, the cloud number concentration increases by 260% and the rain number decreases by 34% in the Set 3 AS simulation as compared to NS, and the MVD is reduced by 38% from 21.3 to 13.2 μm (Table 2). The accretion and autoconversion rates are again shifted in time like Set 1 and their magnitudes are comparable (Fig. 9l). The accretion to autoconversion ratios are 58 and 17 for the Set 3 AS and NS simulations, respectively, larger values than for Set 2, but smaller than for Set 1 (Table 2). Overall the moist sounding in Set 3 creates a convective system with the largest up- and downdrafts with additional cloud water and the most precipitation out of all three simulation sets.

5. Comparison with observations

Before discussing the mechanisms behind the simulation differences, we determine which simulation best matches the DOMEX field campaign observations. Table 3 has been constructed to compare the simulations to the observations. Rain statistics (point max and area mean), cloud-top height, QV, LWC, MVD, and aerosol and cloud number concentrations are included for RF7, a low-wind day during DOMEX. "Point max" is the maximum amount of accumulated rainfall in any one location over the island, "area mean" is the mean accumulated rainfall over the island area, and "rain rate" is computed from the model as the slope of the best fit line to cumulative precipitation amount during hours 6–10. Both "area mean" and "rain rate" are derived from the traces of Figs. 9a–c. Rain observations are computed from the TFFR radar on Guadeloupe (Fig. 6a) from the same day RF7 was flown. The model cloud-top heights are computed as the average maximum height in the model with nonzero liquid water and observational cloud-top heights are from Watson et al. (2015), who used an average cloud-top height value from multiple overisland flights observed by the Wyoming Cloud Radar. Overisland aircraft measurement occurred at 1.8-km height in the early afternoon so mean values from the model at 1.8 km are averaged over the time of peak convection (hours 6–10) to directly compare with the overisland aircraft averages. The two weak wind days (RF7 and RF8) observed during DOMEX had wind speeds around $2\,m\,s^{-1}$ and a relatively dry midtroposphere (Fig. 4a). With the hypothesized surface aerosol source and the dry cloud layer, conditions were most similar to the Set 2 AS simulation so the aircraft observations and Set 2 AS are bolded for emphasis in Table 3.

First, it is clear that the differences between simulations with differing wind speed and cloud-layer moisture overwhelm any differences due to aerosol surface source changes in Table 3. The Set 1 pair has little difference in precipitation and cloud-top height but compared to observations, it precipitates far too heavily. The small difference in precipitation is despite its strong microphysical differences. Table 3 clearly shows the trends previously described. For all simulation sets, an increased aerosol surface source leads to an increase in cloud number concentration, a decrease in MVD, and an increase in LWC due to additional liquid water stored in cloud. This is especially visible in Set 2, which has a

TABLE 3. Precipitation (point max, island mean, and rain rate), cloud-top height, QV, LWC, and microphysical quantities (MVD, aerosol, and cloud number concentration) from observations on RF7, a low-wind day (from Météo-France Guadeloupe TFFR radar and the UWKA aircraft in situ probes and WCR) and the six WRF Model simulations. The microphysical values from the model are averages at 1.8-km height for hours 6–10 during the time of peak convection. The observations and Set 2 AS are in bold for emphasis.

		Precipitation						Microphysics		
	Aerosol	Point max (mm)	Area mean (mm)	Rate (mm hr^{-1})	Cloud top (km)	QV (g kg^{-1})	LWC (g m^{-3})	MVD (μm)	Aerosol number (cm^{-3})	Cloud number (cm^{-3})
Observations		**8**	**0.16**	**—**	**2.8**	**8.1**	**0.65**	**16.5**	**335**	**327**
Set 1	AS	63	1.90	0.427	3.8	8.7	0.46	16.8	420	246
	NS	60	2.07	0.451	4.0	8.7	0.33	26.5	131	77
Set 2	**AS**	**11.5**	**0.07**	**0.019**	**3.1**	**7.2**	**0.65**	**17.3**	**349**	**424**
	NS	9	0.11	0.261	3.0	7.2	0.61	24.3	125	134
Set 3	AS	36	2.43	0.439	4.3	11.2	0.37	16.1	304	211
	NS	81	2.10	0.317	4.0	11.2	0.33	29.3	100	70

significant reduction in precipitation and an increase in cloud LWC. Set 3 has the most precipitation and cloud-top heights that rival the Set 1 simulations. The rain maximas in the Set 3 pair differ the most as a result of a continuous rainshaft that forms over the largest peak in the Set 3 NS simulation.

Encouragingly, precipitation in Set 2 matches best with observations. From a precipitation and cloud-top height perspective, Set 2 NS matches slightly better than Set 2 AS, but differences are small and not significantly distinguishable. Microphysically, Set 2 AS stands out as a much better match to the observations than Set 2 NS. Set 2 NS has an MVD that is significantly larger than observed (24.3 vs 16.5 μm observed), as well as aerosol and cloud number concentrations significantly lower than observed (125 and 134 cm^{-3} respectively vs 335 and 327 cm^{-3} observed). Considering the combination of both precipitation and microphysical aspects, the Set 2 AS simulation is chosen as the best case for comparison to observations.

With confidence in the model results, we can now take a deeper look at the Set 2 AS simulation to gain insight into the observations. Figure 10 includes four panels with cloud microphysical properties averaged along the width of the island whose maximum elevation along the north–south cross section is shown. A black line is included at the aircraft flight elevation of 1.8 km to show the comparable height in the model. The aircraft altitude appears to intersect near the top of the aerosol plume and in the upper half of the cloud region. Microphysically, cloud below aircraft level has higher cloud number concentrations, lower liquid water contents, and smaller cloud droplet diameters with respect to the cloud above aircraft level (Fig. 10).

The surface sourced aerosol in Set 2 AS appears to have filled the air surrounding the island (Fig. 10). We hypothesize that it has both been lofted into the convection from the surface heating, in addition to having been detrained by cloud. Approximately one-third the number of aerosols activated as cloud droplets are later detrained by evaporation of cloud droplets. These lofted and detrained aerosols further accumulate over the island and cannot be distinguished in the model from the aerosols that have not been processed by cloud.

From Fig. 10 it is clear that a surface aerosol source in thermally driven convection can be lofted from the boundary layer into the convection up to heights that were measured by aircraft giving further confidence that the aerosols observed during DOMEX at 1.8 km were from a surface-based source.

6. Discussion and conclusions

Observations from the DOMEX field campaign show that vigorous convection develops over the island of Dominica on all days, but despite the vigorous convection, not all days precipitate heavily. Days with little rain see a dramatic increase in cloud number concentration, a reduced cloud MVD, and massive detrainment of aerosols. This might suggest an aerosol impact on precipitation but we conclude otherwise. In addition to the cloud microphysical changes, days without rain have a relatively dry cloud layer and we find the impacts of this dryness on precipitation dominate over aerosol impacts. Environmental conditions ultimately place stronger controls on precipitation than do aerosols.

The Set 1 simulations have no wind imposed on the domain while the Set 2 simulations have a 2 $m\,s^{-1}$ background wind speed. Both sets have a relatively dry cloud layer. The addition of wind to Set 2 is important for creating a realistic environment and causes significant changes: wind ventilates the overisland region, reducing the aerosol number concentration, the dominance of cloud droplet scavenging (accretion), and the humidity (QV in Table 3). With wind, the residence time of air over the island is shortened, which causes

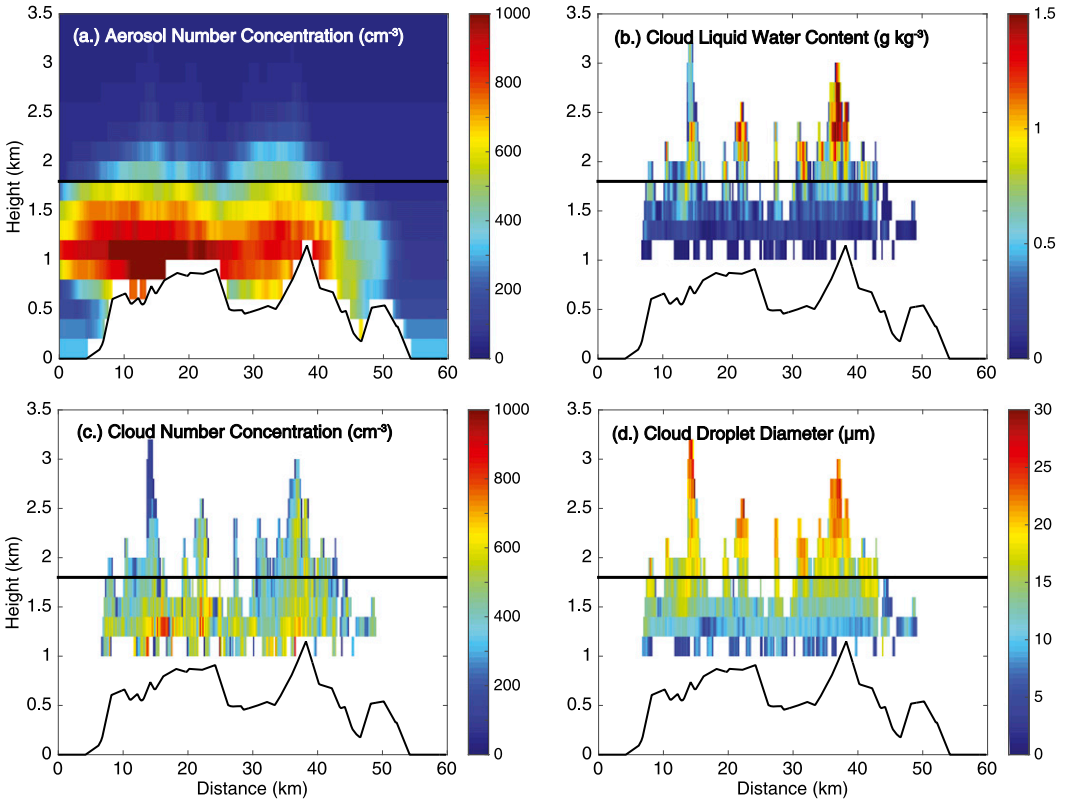

FIG. 10. Two-dimensional slices (from south to north) averaged over the island width from the Set 2 AS simulation at 7 h during the time of peak convection for (a) aerosol number concentration (cm^{-3}), (b) cloud liquid water content ($g\,kg^{-1}$), (c) cloud number concentration (cm^{-3}), and (d) cloud droplet diameter (μm). A line at 1.8-km height helps to compare the height measured by aircraft with these model results and the maximum island elevation in the model along the slice is shown.

the cloud-top height to decrease because the clouds that form grow vertically into consistently drier air that has not been preconditioned for convection. Also, all measures of precipitation in Table 3 for Set 2 decrease as a result of both the decreased cloud-top height and the decreased prevalence of accretion. Set 1 simulations have the highest accretion to autoconversion ratios owing to their symmetric and stationary convective system, which decreases the impact of aerosols.

The Set 2 simulations have a relatively dry cloud layer while the Set 3 simulations have a moist cloud layer. Both sets have a $2\,m\,s^{-1}$ wind speed and therefore the equivalent overisland ventilation. The increased moisture in the cloud layer in Set 3 causes significant changes: cloud-top heights increase, dry-air entrainment is reduced, and a continuous source of moisture is supplied. These cause the convection to invigorate and through the additional cloud formation and latent heating, all measures of convective strength and precipitation increase. A combination of heavy precipitation (which scavenges aerosol) and rapid updrafts (which activates additional aerosol; e.g., Russotto et al. 2013) brings the Set 3 aerosol number concentration to its lowest and the MVD difference to its largest (Table 3). Despite the large microphysical impact, the high rate of precipitation in the moist atmosphere of Set 3 decreases aerosol sensitivity.

While there is a clear dominance of wind and moisture, the aerosol surface source also has an impact on precipitation. Simulations with an aerosol surface source precipitate later, have higher cloud liquid water contents, higher cloud and lower rain number concentration, and smaller cloud droplet diameters. Also, while accretion always dominates over autoconversion, a surface aerosol source decreases the rate of autoconversion, thereby further increasing the accretion dominance.

While some aerosol impacts were consistent among the simulation sets, some impacts were modulated by the changes in wind and moisture. Set 1 and Set 3 simulations were most similar to each other; they both had peaks in cloud water content in their AS simulations that were shifted in time compared to their NS simulations (Figs. 9d and 9f), and the same with the rate of rain formation (Figs. 9j and 9l). The most significant difference is that the convection in Set 3 outlasts the forcing while the convection in Set 1 decreases with it (Figs. 9d

and 9f). We argue that this determines whether the NS (as in Set 1) or the AS (as in Set 3) simulation precipitates the most (Fig. 9a vs Fig. 9c).

In both Set 1 and Set 3 simulation pairs, cloud water builds and after precipitation begins, it is rapidly converted to rainwater. In both, the cloud liquid water in the AS simulations continues to grow after the surface heating peaks at hour 6 (Figs. 9d and 9f). Additional cloud liquid water, and the higher cloud tops in Set 1 and 3 AS simulations is evidence for convective invigoration from delayed precipitation formation. Additional water is stored as cloud water such that it is available for later rainout. The delayed rainout allows the AS simulations to ''catch up'' to the NS simulations even after the initial delay. The timing here is everything; depending on how much cloud water can build and rain out after heating has peaked determines whether precipitation in the AS simulation will exceed the amount of precipitation in the NS simulation. In Set 1, the high dominance of accretion and the relatively dry atmosphere cause the convective system to dissipate rapidly as the heating weakens (Fig. 9d). After heating dies down, with no background wind speed, circulation shuts down, the symmetric system rapidly rains out depleting the cloud water, and little additional moisture is added to continue convection. Set 3 has a different fate. A light wind continues to bring a source of moisture from the moist atmosphere and even after all surface heating has ceased, cloud water is still present (Fig. 9f). This is true not just for Set 3 AS, but also Set 3 NS, which also has continuous available moisture. It appears that the boundary between inhibiting and enhancing precipitation with aerosol is a fine line and depends heavily on the wind speed, the atmospheric moisture content, and the strength of the convective system, including the strength and timing of the forcing.

Overall, Sets 1 and 3 had little aerosol impact compared to Set 2. Set 2 had a 37% reduction in precipitation from NS to AS [comparable to Lynn et al. (2007)] as compared to an 8% reduction and a 16% increase for Sets 1 and 3, respectively. The combination of wind ventilation and a relatively dry cloud layer in Set 2 resulted in little precipitation overall, 74%–97% less than Sets 1 and 3 and it is because of the little precipitation that the relative difference between the Set 2 pair due to aerosol surface source is large.

In Set 2, instead of the rate of accretion being shifted in time like Set 1 and 3, Set 2 AS has a similar timing but a smaller magnitude than Set 2 NS (Fig. 9k). The ratio of accretion to autoconversion in Set 2 is the lowest of all simulation sets showing the strong role of autoconversion when precipitation is light. The differences in precipitation are especially interesting alongside the similarities in the cloud dynamics. Cloud-top heights and vertical velocities (Fig. 9h) have smaller differences than both Sets 1 and 3. Aerosols are having an impact on Set 2 simulations, not by invigorating convection and changing dynamics, but by making precipitation formation less efficient through the modification of cloud microphysics. The case where aerosols have the largest impact is the case with the weakest forcing.

We believe that the DOMEX observations constitute one of the clearest examples of surface aerosols getting into and having an impact on cloud microphysics. In spite of the clear observed microphysical impacts, wind and cloud-layer moisture have a stronger effect on precipitation in this case of tropical orographic cumulus convection. The effect of aerosol is diminished by the dominance of accretion.

Acknowledgments. The authors acknowledge funding from the National Science Foundation (NSF Grant 0930356 and AGS-1431053) and NCAR's Advanced Study Program; helpful discussions with Trude Eidhammer, Trude Storelvmo, William R. Boos, Chun-Chih Wang, Daniel J. Kirshbaum, Justin R. Minder, Jeffrey R. French, and Jørgen B. Jensen; and constructive comments from three anonymous reviewers. We also acknowledge the Yale University High Performance Computing Center, Brian Dobbins in particular, for their support with modeling.

REFERENCES

Ackerman, A. S., M. P. Kirkpatrick, D. E. Stevens, and O. B. Toon, 2004: The impact of humidity above stratiform clouds on indirect aerosol climate forcing. *Nature*, **432**, 1014–1017, doi:10.1038/nature03174.

Adams, P. J., and J. H. Seinfeld, 2002: Predicting global aerosol size distributions in general circulation models. *J. Geophys. Res.*, **107**, 4370, doi:10.1029/2001JD001010.

Albrecht, B., 1989: Aerosols, cloud microphysics, and fractional cloudiness. *Science*, **245**, 1227–1230, doi:10.1126/science.245.4923.1227.

Bert, L. K., C. M. Berkowitz, J. C. Barnard, G. Senum, and S. R. Springston, 2011: Observations of the first aerosol indirect effect in shallow cumuli. *Geophys. Res. Lett.*, **38**, L03809, doi:10.1029/2010GL046047.

Boucher, O., and Coauthors, 2013: Clouds and aerosols. *Climate Change 2013: The Physical Science Basis*, T. F. Stocker et al., Eds., Cambridge University Press, 571–657.

Breon, F.-M., D. Tanre, and S. Generoso, 2002: Aerosol effect on cloud droplet size monitored from satellite. *Science*, **295**, 834–838, doi:10.1126/science.1066434.

Cai, Y., J. R. Snider, and P. Wechsler, 2013: Calibration of the passive cavity aerosol spectrometer probe for airborne determination of the size distribution. *Atmos. Meas. Tech.*, **6**, 2349–2358, doi:10.5194/amt-6-2349-2013.

Costantino, L., and F.-M. Breon, 2013: Aerosol indirect effect on warm clouds over South-East Atlantic, from co-located MODIS and *CALIPSO* observations. *Atmos. Chem. Phys.*, **13**, 69–88, doi:10.5194/acp-13-69-2013.

Damiani, R., and Coauthors, 2008: The cumulus, photogrammetric, in situ, and Doppler observations experiment of 2006. *Bull. Amer. Meteor. Soc.*, **89**, 57–73, doi:10.1175/BAMS-89-1-57.

Durkee, P. A., and Coauthors, 2000: Composite ship track characteristics. *J. Atmos. Sci.*, **57**, 2542–2553, doi:10.1175/1520-0469(2000)057<2542:CSTC>2.0.CO;2.

Fan, J., R. Zhang, G. Li, and W.-K. Tao, 2007: Effects of aerosols and relative humidity on cumulus clouds. *J. Geophys. Res.*, **112**, D14204, doi:10.1029/2006JD008136.

Feingold, G., W. L. Eberhard, D. E. Veron, and M. Previdi, 2003: First measurements of the Twomey indirect effect using ground-based remote sensors. *Geophys. Res. Lett.*, **30**, 1287, doi:10.1029/2002GL016633.

Grant, L. D., and S. C. van den Heever, 2014: Microphysical and dynamical characteristics of low-precipitation and classic supercells. *J. Atmos. Sci.*, **71**, 2604–2624, doi:10.1175/JAS-D-13-0261.1.

Huang, H., G. E. Thomas, and R. G. Grainger, 2010: Relationship between wind speed and aerosol optical depth over remote ocean. *Atmos. Chem. Phys.*, **10**, 5943–5950, doi:10.5194/acp-10-5943-2010.

Kaufman, Y. J., and T. Nakajima, 1993: Effect of Amazon smoke on cloud microphysics and albedo-analysis from satellite imagery. *J. Appl. Meteor.*, **32**, 729–744, doi:10.1175/1520-0450(1993)032<0729:EOASOC>2.0.CO;2.

Khain, A., D. Rosenfend, and A. Pokrovsky, 2005: Aerosol impact on the dynamics and microphysics of deep convective clouds. *Quart. J. Roy. Meteor. Soc.*, **131**, 2639–2663, doi:10.1256/qj.04.62.

Klemp, J. B., J. Dudhia, and A. D. Hassiotis, 2008: An upper gravity-wave absorbing layer for NWP applications. *Mon. Wea. Rev.*, **136**, 3987–4004, doi:10.1175/2008MWR2596.1.

Klett, D., and M. H. Davis, 1973: Theoretical collision efficiencies of cloud droplets at small Reynolds numbers. *J. Atmos. Sci.*, **30**, 107–117, doi:10.1175/1520-0469(1973)030<0107:TCEOCD>2.0.CO;2.

Knievel, J. C., G. H. Bryan, and J. P. Hacker, 2007: Explicit numerical diffusion in the WRF Model. *Mon. Wea. Rev.*, **135**, 3808–3824, doi:10.1175/2007MWR2100.1.

Lohmann, U., and J. Feichter, 2005: Global indirect aerosol effects: A review. *Atmos. Chem. Phys.*, **5**, 715–737, doi:10.5194/acp-5-715-2005.

Lynn, B., A. Khain, D. Rosenfeld, and W. L. Woodley, 2007: Effects of aerosols on precipitation from orographic clouds. *J. Geophys. Res.*, **112**, D10225, doi:10.1029/2006JD007537.

Mapes, B. E., and P. Zuidema, 1996: Radiative-dynamical consequences of dry tongues in the tropical troposphere. *J. Atmos. Sci.*, **53**, 620–638, doi:10.1175/1520-0469(1996)053<0620:RDCODT>2.0.CO;2.

Minder, J. R., R. B. Smith, and A. D. Nugent, 2013: The dynamics of ascent-forced orographic convection in the tropics: Results from Dominica. *J. Atmos. Sci.*, **70**, 4067–4088, doi:10.1175/JAS-D-13-016.1.

Muhlbauer, A., and U. Lohmann, 2008: Sensitivity studies of the role of aerosols in warm-phase orographic precipitation in different dynamical flow regimes. *J. Atmos. Sci.*, **65**, 2522–2542, doi:10.1175/2007JAS2492.1.

Nugent, A. D., and R. B. Smith, 2014: Initiating moist convection in an inhomogeneous layer by uniform ascent. *J. Atmos. Sci.*, **71**, 4597–4610, doi:10.1175/JAS-D-14-0089.1.

——, J. R. Minder, and R. B. Smith, 2014: Wind speed control of tropical orographic convection. *J. Atmos. Sci.*, **71**, 2695–2712, doi:10.1175/JAS-D-13-0399.1.

Nuijens, L., B. Stevens, and A. P. Siebesma, 2009: The environment of precipitating shallow cumulus convection. *J. Atmos. Sci.*, **66**, 1962–1979, doi:10.1175/2008JAS2841.1.

Parsons, D. B., J.-L. Redelsperger, and K. Yoneyama, 2000: The evolution of the tropical western Pacific atmosphere–ocean system following the arrival of a dry intrusion. *Quart. J. Roy. Meteor. Soc.*, **126**, 517–548, doi:10.1002/qj.49712656307.

Roe, G. H., 2005: Orographic precipitation. *Annu. Rev. Earth Planet. Sci.*, **33**, 645–671, doi:10.1146/annurev.earth.33.092203.122541.

Rogers, R. R., and M. K. Yau, 1989: *Short Course in Cloud Physics.* 3rd ed. Butterworth-Heinemann, 304 pp.

Rosenfeld, D., 1999: TRMM observed first direct evidence of smoke from forest fires inhibiting rainfall. *Geophys. Res. Lett.*, **26**, 3105–3108, doi:10.1029/1999GL006066.

Russotto, R. D., T. Storelvmo, and R. B. Smith, 2013: Modeling aerosol activation in a tropical, orographic, island setting: Sensitivity tests and comparison with observations. *Atmos. Res.*, **134**, 12–23, doi:10.1016/j.atmosres.2013.07.017.

Saleeby, S. M., S. R. Herbener, and S. C. van den Heever, 2015: Impacts of cloud droplet–nucleating aerosols on shallow tropical convection. *J. Atmos. Sci.*, **72**, 1369–1385, doi:10.1175/JAS-D-14-0153.1.

Skamarock, W. C., and Coauthors, 2008: A description of the Advanced Research WRF version 3. NCAR Tech. Note NCAR/TN-475+STR, 113 pp., doi:10.5065/D68S4MVH.

Smith, R. B., and Coauthors, 2012: Orographic precipitation in the tropics: The Dominica Experiment. *Bull. Amer. Meteor. Soc.*, **93**, 1567–1579, doi:10.1175/BAMS-D-11-00194.1.

Stevens, B., 2005: Atmospheric moist convection. *Annu. Rev. Earth Planet. Sci.*, **33**, 605–643, doi:10.1146/annurev.earth.33.092203.122658.

——, and A. Seifert, 2008: Understanding macrophysical outcomes of microphysical choices in simulations of shallow cumulus convection. *J. Meteor. Soc. Japan*, **86A**, 143–162, doi:10.2151/jmsj.86A.143.

Storer, R. L., S. C. van den Heever, and G. L. Stephens, 2010: Modeling aerosol impacts on convective storms in different environments. *J. Atmos. Sci.*, **67**, 3904–3915, doi:10.1175/2010JAS3363.1.

Thompson, G., and T. Eidhammer, 2014: A study of aerosol impacts on clouds and precipitation development in a large winter cyclone. *J. Atmos. Sci.*, **71**, 3636–3658, doi:10.1175/JAS-D-13-0305.1.

Twomey, S., 1974: Pollution and the planetary albedo. *Atmos. Environ.*, **8**, 1251–1256, doi:10.1016/0004-6981(74)90004-3.

——, and J. Warner, 1967: Comparison of measurements of cloud droplets and cloud nuclei. *J. Atmos. Sci.*, **24**, 702–703, doi:10.1175/1520-0469(1967)024<0702:COMOCD>2.0.CO;2.

Wang, C.-C., and D. J. Kirshbaum, 2015: Thermally forced convection over a mountainous tropical island. *J. Atmos. Sci.*, **72**, 2484–2506, doi:10.1175/JAS-D-14-0325.1.

Warner, J., and S. Twomey, 1967: The production of cloud nuclei by cane fires and the effect on cloud droplet concentration. *J. Atmos. Sci.*, **24**, 704–706, doi:10.1175/1520-0469(1967)024<0704:TPOCNB>2.0.CO;2.

Watson, C. D., R. B. Smith, and A. D. Nugent, 2015: Shallow, orographically triggered convection over Dominica: Observations from DOMEX. *J. Atmos. Sci.*, **72**, 3051–3072, doi:10.1175/JAS-D-14-0333.1.

Xiao, H., Y. Yin, L. Jin, Q. Chen, and J. Chen, 2014: Simulation of aerosol effects on orographic clouds and precipitation using WRF Model with a detailed bin microphysics scheme. *Atmos. Sci. Lett.*, **15**, 134–139, doi:10.1002/asl2.480.

Zehnder, J. A., J. Hu, and A. Radzan, 2009: Evolution of the vertical thermodynamic profile during the transition from shallow to deep convection during CuPIDO 2006. *Mon. Wea. Rev.*, **137**, 937–953, doi:10.1175/2008MWR2829.1.

Zubler, E. M., U. Lohmann, D. Lüthi, and C. Schär, 2011: Statistical analysis of aerosol effects on simulated mixed-phase clouds and precipitation in the Alps. *J. Atmos. Sci.*, **68**, 1474–1492, doi:10.1175/2011JAS3632.1.